


Controlled Release of TGF- β 3 for Effective Local Endogenous Repair in IDD Using Rat Model

Lifan Zhu^{1,2,*}, Yanjun Yang^{1,*}, Zhanjun Yan^{1,*}, Jincui Zeng¹, Fengbiao Weng¹, Yuhui Shi¹, Pengcheng Shen¹, Ling Liu², Huilin Yang¹

¹Department of Orthopedics, Suzhou Ninth Hospital Affiliated to Soochow University, Suzhou, 215200, People's Republic of China; ²Department of Orthopedics, The First Affiliated Hospital of Soochow University, Suzhou, 215200, People's Republic of China

*These authors contributed equally to this work

Correspondence: Huilin Yang, Department of Orthopedics, The First Affiliated Hospital of Soochow University, 188 Shizi Street, Suzhou, 215006, People's Republic of China, Email suzhouspine@163.com; Lifan Zhu, Department of Orthopedics, Suzhou Ninth Hospital affiliated to Soochow University, Suzhou, 215200, People's Republic of China, Email zhulifan201608@163.com

Introduction: Intervertebral disc (IVD) degeneration (IDD) is one of the most widespread musculoskeletal diseases worldwide and remains an intractable clinical challenge. Currently, regenerative strategies based on biomaterials and biological factors to facilitate IVD repair have been widely explored. However, the harsh microenvironment, such as increased ROS and acidity, of the degenerative region impedes the efficiency of IVD repair. Here, an intelligent biodegradable nanoplatform using hollow manganese dioxide (H-MnO₂) was developed to modulate the degenerative microenvironment and release transforming growth factor beta-3 (TGF- β 3), which may achieve good long-term therapeutic effects on needle puncture-induced IDD.

Methods: Surface morphology and elemental analysis of the MnO₂ nanoparticles (NPs) were performed by transmission electron microscopy and an energy-dispersive X-ray spectroscopy detector system, respectively. The biological effects of MnO₂ loaded with TGF- β 3 (TGF- β 3/MnO₂) on nucleus pulposus cells (NPCs) were assessed via cytoskeleton staining, EdU staining, qPCR and immunofluorescence. The efficacy of TGF- β 3/MnO₂ on needle puncture-induced IDD was further examined using MRI and histopathological and immunohistochemical staining.

Results: The MnO₂ NPs had a spherical morphology and hollow structure that dissociated in the setting of a low pH and H₂O₂ to release loaded TGF- β 3 molecules. In the oxidative stress environment, TGF- β 3/MnO₂ was superior to TGF- β 3 and MnO₂ NPs in the suppression of H₂O₂-induced matrix degradation, ROS, and apoptosis in NPCs. When injected into the IVDs of a rat IDD model, TGF- β 3/MnO₂ was able to prevent the degeneration and promote self-regeneration.

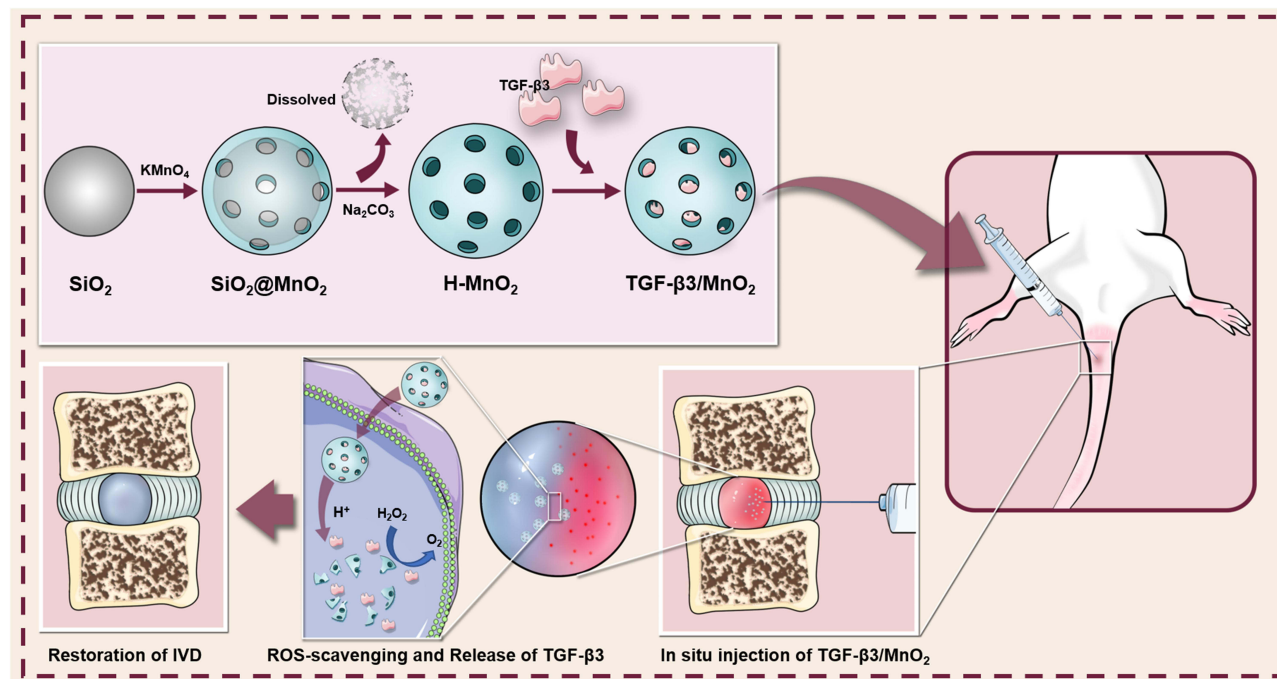
Conclusion: Use of an MnO₂ nanoplatform for biological factors release to regulate the IDD microenvironment and promote endogenous repair may be an effective approach for treating IDD.

Keywords: intervertebral disc degeneration, hollow manganese dioxide, transforming growth factor beta-3, oxidative stress, endogenous repair

Introduction

Low back pain, a leading cause of disability worldwide, is strongly associated with intervertebral disc degeneration (IDD), with IDD appearing in 40% of all cases of lower back pain.¹⁻³ The loss of disc cell viability and functionality is thought to be critical to disrupting disc homeostasis.⁴ Excessive apoptosis and cellular senescence from IDD contribute to a reduced number of viable disc cells.^{5,6} Deficiencies in anabolic factors such as transforming growth factor beta (TGF- β) and insulin-like growth factor-1 may further reduce cellular viability and the production of extracellular matrix (ECM).⁷ In addition, the increased production of reactive oxygen species (ROS) and catabolic cytokines along with the accumulation of senescent disc cells may further deteriorate the microenvironment of degenerated intervertebral discs (IVDs).⁸ Based on these observations, the ideal biological therapeutics for IVD regeneration should provide the disc with viable and functional cells and improve the survival conditions within degenerating IVDs.⁹

Graphical Abstract



TGF- β 3, an important member of the TGF- β superfamily, is involved in the regulation of biological processes such as proliferation, survival, and differentiation.^{10,11} TGF- β 3 upregulates the expression of genes involved in cartilage formation to promote cartilage repair and accelerate chondrogenic differentiation.¹² TGF- β 3 was shown to stimulate adipose-derived stem cell proliferation and chondrogenic differentiation *in vitro*.¹³ Importantly, TGF- β 3 stimulation enhances cell survival and matrix deposition in the IVDs.^{14,15} Hence, targeting the supply of TGF- β 3 could improve the metabolic imbalance of the ECM in IDD, and potentially slow its progression. However, supplying pure TGF- β 3 to diseased tissues will cause local overdose, and the protein will be quickly washed away or degraded by body fluids.¹⁰ A way to deliver a sustained dose of TGF- β 3 into target tissues could facilitate the IVD repair process.

Nanoparticles (NPs) have been developed as carriers for the delivery of a wide range of active pharmaceutical ingredients to overcome the limitations of free therapeutics and navigate biological barriers.¹⁶ Encapsulation in NPs can improve the stability and solubility of the cargo, promote transmembrane transport, and prolong drug circulation time, thereby increasing its safety and effectiveness.¹⁷ In recent years, manganese dioxide (MnO_2)-based NPs have attracted interest in the field of medical science due to their high sensitivity to H_2O_2 and H^+ , which are abundant in the tumor, osteoarthritis, and IDD microenvironments.^{18–20} Yang et al developed a hollow MnO_2 nanoplatform for the sustained release of anti-tumor drugs in a slightly acidic environment and in the presence of H_2O_2 .²¹ Kumar et al reported that MnO_2 NPs protect cartilage from inflammation induced by oxidative stress.²² However, little is known about the involvement of MnO_2 NPs in the regulation of the IDD microenvironment. During IDD pathogenesis, the acidity and ROS levels within the degenerated IVDs significantly increase, which can inhibit normal cellular activity and accelerate IVD degeneration.^{9,23,24} Therefore, the application of MnO_2 NPs might improve the harsh survival conditions in the disc microenvironment as a way to promote tissue regeneration.

In this study, we prepared an intelligent drug delivery system based on hollow MnO_2 NPs encapsulating TGF- β 3. The NPs exhibited satisfactory drug loading efficiency along with pH-responsive degradation. The hollow MnO_2 NPs degraded to release the encapsulated TGF- β 3 when exposed to excessive H_2O_2 and/or H^+ in tissues and cells. The released TGF- β 3 improved cell survival and ECM deposition by scavenging ROS, thereby alleviating the progression of

IDD. Based on these results, the hollow MnO₂-based responsive nanocarriers for drug delivery show promise for IVD repair.

Materials and Methods

Synthesis and Characterization of Hollow MnO₂ Nanoparticles

Hollow MnO₂ NPs were prepared as previously described.^{21,25} Briefly, solid SiO₂ (sSiO₂) NPs were first synthesized as follows: 14 mL of ethanol, 2 mL of deionized water, and 500 μL of NH₃·H₂O were mixed in a 50-mL round-bottom flask. The mixture was heated under magnetic stirring in an oil bath at 50 °C for 5 min. 500 μL of tetraethyl orthosilicate was then added dropwise and the mixture was stirred at 50 °C for 2 h to produce sSiO₂ NPs. The resulting sSiO₂ NPs were washed twice with ethanol and twice with water and then stored in water for further use. For the synthesis of sSiO₂@MnO₂ NPs, 600 mg of KMnO₄ dispersed in 20 mL of water was added dropwise into the sSiO₂ NPs during sonication. The mixture was ultrasonicated for 1 h, then stirred overnight at room temperature. The resulting sSiO₂@MnO₂ NPs were washed three times with deionized water and centrifuged at 14,800 rpm/min. Finally, the prepared sSiO₂ coated with mesoporous MnO₂ was dissolved in Na₂CO₃ at 60 °C for 12 h. The resulting hollow MnO₂ NPs were then centrifuged and washed several times with water. The surface morphology and elemental analysis of the NPs were determined by transmission electron microscopy (TEM; FEI Tecnai F20, Hillsboro, OR, USA) and an energy-dispersive X-ray spectroscopy detector system (EDS, Oxford X-MAX, Oxford, UK), respectively.

Encapsulation of TGF-β3 into Hollow MnO₂ Nanoparticles

For TGF-β3 loading, hollow MnO₂ NPs (5 mg) were added into 1 mL of phosphate-buffered saline (PBS; pH 7.4) containing TGF-β3 (1 μg; Sigma-Aldrich, St. Louis, MO, USA) and stirred for 12 h at room temperature. Subsequently, the NPs were centrifuged, and the supernatant was removed.

Examination of in-vitro Release of TGF-β3 from MnO₂ Nanoparticles

The release of TGF-β3 from the NPs in vitro was quantified by ELISA (Sangon Biotech, Shanghai, China). The NPs were incubated in 1 mL of PBS at different pH values (6.5 and 7.4) in the absence or presence of 100 μM H₂O₂. At predetermined time points, the samples were centrifuged, the supernatant was collected, and an equal amount of fresh PBS was added to continue the release process. All collected solutions were kept frozen at -20°C for subsequent analysis with TGF-β3-ELISA.

Isolation and Culture of Nucleus Pulposus Cells

To isolate nucleus pulposus cells (NPCs), six-week-old male Sprague-Dawley rats were sacrificed and their lumbar and caudal IVDs were harvested under aseptic conditions. We then separated gel-like nucleus pulposus tissues from the discs and treated them with 0.25% (w/v) type II collagenase (Yeasen, Shanghai, China) for 4 h at 37 °C. The obtained cell suspension was centrifuged at 1200 rpm for 3 min and then cultured with DMEM/F12 containing 10% fetal bovine serum (HyClone, Logan, UT, USA) and 1% penicillin/streptomycin (Gibco, Grand Island, NY, USA) in a humidified incubator at 37 °C with 5% CO₂. NPCs at passage 2 were used for all of the experiments in this study.

Cell Culture

NPCs at passage 2 were plated on a cell culture dish at an initial density of 5000 cells/cm². When the cells were attached, H₂O₂ solution was diluted with DMEM/F12 medium and then added into the dishes to a final concentration of 100 μM to induce oxidative stress in the NPCs. To further investigate whether NPs altered oxidative stress, after treatment with H₂O₂ for 12 h, the medium was replenished by fresh medium containing TGF-β3, MnO₂, and TGF-β3/MnO₂ for 24 h, respectively.

In vitro Cytotoxicity Assay

The cell toxicity of the NPs was determined by examining the viability of NPCs treated with NPs using a CCK-8 assay (NCM Biotech, Suzhou, China). Briefly, cells (5×10³ per well) were seeded into 96-well plates and cultured for 12 h to

allow cell attachment. The cells were then incubated with a series of increasing concentrations of hollow MnO₂ NPs for 24 h. After incubation, the cell medium was removed and replaced with 100 µL of culture medium and 10 µL of CCK-8 reagent for another 2 h for color development. Optical density was measured using a microplate reader (BioTek, VT, USA) at 450 nm.

Cellular Uptake Experiments

To assess the cellular uptake efficiency of the NPs, bovine serum albumin (BSA), and fluorescein isothiocyanate-labeled BSA (FITC-BSA; Solarbio, Beijing, China) were encapsulated into hollow MnO₂ NPs. After encapsulation, NPCs (5×10³ per well) were cultured in 48-well plates at 37 °C for 12 h. After complete adhesion, the cells were washed twice with PBS followed by the addition of 100 µL of fresh medium containing NPs loaded with BSA or FITC-BSA. Incubation was then continued for 12 h. Next, the cells were washed three times with PBS to remove the residual NPs, fixed with 4% paraformaldehyde solution for 15 min, and stained with TRITC-phalloidin and DAPI. Finally, images were obtained using a fluorescence microscope.

Intracellular ROS Assay

An ROS assay kit (Beyotime, Shanghai, China) was used to measure the accumulation of intracellular ROS in the treated cells. The cells were first exposed to DCFH-DA solution (10 µM) and then incubated for 1 h at 37 °C. After a wash with PBS, the fluorescence of the cells was observed with a fluorescence microscope.

Cell Proliferation Assay

Cell proliferation was measured using a BeyoClick™ EdU Cell Proliferation Kit with Alexa Fluor 488 (Beyotime, Shanghai, China). Briefly, immediately before H₂O₂ treatment in all groups, EdU was added to label cells undergoing active DNA synthesis. After 6 h, the cells were fixed in 4% paraformaldehyde for 15 min and permeabilized with 0.3% Triton X-100 in PBS for 10 min. Subsequently, the samples were incubated with click reaction solution at room temperature for 30 min, and the nuclei were counterstained with Hoechst 33342 dye. Images were acquired using a fluorescence microscope.

Quantitative Polymerase Chain Reaction Analysis

TRIzol reagent (Invitrogen, Carlsbad, CA, USA) was used to extract the total RNA from NPCs under different conditions. The RNA concentrations were measured using a NanoDrop 2000 spectrophotometer (Thermo Fisher Scientific, Waltham, MA, USA). RNA (1 µg) was reverse-transcribed into cDNA using a 5X All-In-One RT MasterMix (abm, Vancouver, BC, Canada) according to the manufacturer's instructions. Subsequently, qPCR was performed using iQ SYBR Green Supermix (Bio-Rad, Hercules, CA, USA). The primer sequences (Sangon Biotech, Shanghai, China) of the genes used in this study are listed in Table 1. The expression of each gene was normalized by the housekeeping gene GAPDH. Relative changes in mRNA level were analyzed using the 2^{-ΔΔCT} method.

Immunofluorescence

NPCs were fixed in 4% paraformaldehyde for 15 min and then permeabilized with 0.3% Triton X-100 in PBS for 10 min. Non-specific binding was blocked by a commercial blocking reagent (Beyotime, Shanghai, China) followed by primary antibodies incubation at 4 °C overnight (rabbit anti-Col-II, rabbit anti-iNOS, Abcam, Cambridge, UK). After overnight incubation, samples were incubated with second antibodies (Beyotime, Shanghai, China) for 1 h. Nuclei were stained with DAPI and images were acquired using a fluorescence microscope. Semi-quantitative fluorescence analysis was performed using Image J software (NIH, Bethesda, MD, USA).

Examination of Caudal Full (Form of IDD) Using Rat Model

All procedures followed the NIH Guide for the Care and Use of Laboratory Animals and were approved by the Institutional Animal Care and Use Committee of Soochow University. After complete anesthesia, the rat tails were disinfected, and Co7-8 IVDs were punctured sequentially with 21G needles to induce degeneration. To ensure that

Table 1 Primers for qPCR

Gene	Forward (5'-3')	Reverse (5'-3')
SOD1	CGGCTTCTGTCGTCTCCTTGC	AACTGGTTCACCGCTTGCCTTC
SOD2	GCTGGAGGCTATCAAGCGTGAC	TTAGAGCAGGCGCAATCTGTAAAG
CAT	GGCCTGACTGACGCGATTGC	CTGCTCCTTCCAAGTCTTCATCTG
Adamts5	TCCTCTTGGTGGCTGACTCTTCC	TGGTTCTCGATGCTTGCATGACTG
MMP3	CAGTCCTGCTGTGGCTGTGTAC	AACCTCCATGCCAGCATCTTCTTC
BAX	CACCAGCTCTGAACAGATCATGA	TCAGCCCATCTTCTTCCAGATGGT
Col-II	ACGCTCAAGTCGCTGAACAACC	ATCCAGTAGTCTCCGCTCTTCCAC
iNOS	GAGACGCACAGGCAGAGGTTG	CAGGAAGGCAGCAGGCACAC
COX-2	TTCCAGTATCAGAACC GCATTGCC	CCGTGTTCAAGGAGGATGGAGTTG
ACAN	GGCGT CCAA CCAAC CCGAG	GGCGT CCAA CCAAC CCGAG
MCL1	TCATCTCCCCTACCTGC	ACTCCACAAACCCATCCC
BCL2	CACCCCTGGCATCTTCTCCTT	AGCGTCTTCAAGAGACAGCCAG
GAPDH	GACATGCCGCCTGGAGAAAC	AGCCAGGATGCCCTTAGT

trauma was induced, a needle was used to puncture the center of the discs, rotated for 5 s then the position maintained for 30s. Each disc was then injected with 20 μ L of material by a 33 G needle; in the negative control group, the discs were injected with PBS instead of NPs. After surgery, the rats were placed in a warm and ventilated location.

Magnetic Resonance Imaging

Four and eight weeks after surgery, the water contents of the IVDs were evaluated on magnetic resonance imaging (MRI, 3.0 T; Siemens, Germany) based on the signal intensity in sagittal T2-weighted images. The MRI images were evaluated by another blinded researcher using the classification for intervertebral disc degeneration (Table 2), as previously reported.²⁶

Histopathological and Immunohistochemical Analysis of Intervertebral Disc Regeneration

After sacrifice, the IVDs were removed from each rat and placed in 10% formalin for 48 h, decalcified in 10% EDTA for 30 d, and then embedded in paraffin blocks. The specimens were cut into 5- μ m-thick histopathological sections followed by staining with either H&E or Safranin-O/Fast Green. The histopathological grade was calculated as described in previous work²⁷ and the specific definition of histopathological grade was shown in Table 3. To observe the expressions of type II collagen and iNOS in the harvested tissues, the sections were immunohistochemically stained for collagen type II and iNOS (Abcam, Cambridge, UK). Semi-quantitative immunohistochemical stain analysis was performed using Image J software.

Table 2 Classification of Disc Degeneration

Grade	Structure	Distinction of Nucleus and Annulus	Signal Intensity	Height of Intervertebral Disc
I	Homogeneous, bright white	Clear	Hyperintense, isointense to cerebrospinal fluid	Normal
II	Inhomogeneous with or without horizontal bands	Clear	Hyperintense, isointense to cerebrospinal fluid	Normal
III	Inhomogeneous, gray	Unclear	Intermediate	Normal to slightly decreased
IV	Inhomogeneous, gray to black	Lost	Intermediate to hypointense	Normal to moderately decreased
V	Inhomogeneous, black	Lost	Hypointense	Collapsed disc space

Table 3 Histological Grading Scale

Category	Grade
I. Cellularity of the annulus fibrosus	1. Fibroblasts comprise more than 75% of the cells 2. Neither fibroblasts nor chondrocytes comprise more than 75% of the cells 3. Chondrocytes comprise more than 75% of the cells
II. Morphology of the annulus fibrosus	1. Well-organized collagen lamellae without ruptured or serpentine fibers 2. Inward bulging, ruptured or serpentine fibers in less than one third of the annulus 3. Inward bulging, ruptured or serpentine fibers in more than one third of the annulus
III. Border between the annulus fibrosus and nucleus pulposus	1. Normal, without any interruption 2. Minimal interruption 3. Moderate or severe interruption
IV. Cellularity of the nucleus pulposus	1. Normal cellularity with stellar shaped nuclear cells evenly distributed throughout the nucleus 2. Slight decrease in the no. of cells with some clustering 3. Moderate or severe decrease (>50%) in the number of cells with all the remaining cells clustered and separated by dense areas of proteoglycans
V. Morphology of the nucleus pulposus	1. Round, comprising at least half of the disc area in midsagittal sections 2. Rounded or irregularly shaped, comprising one quarter to half of the disc area in midsagittal sections 3. Irregularly shaped, comprising less than one quarter of the disc area in midsagittal sections

Statistical Analysis

All data are expressed as mean \pm standard deviation. Statistical significance was evaluated using a one-way analysis of variance (GraphPad Software, USA) with Tukey's multiple comparison test to further evaluate differences between groups. *P* values less than 0.05 were considered statistically significant.

Results

Synthesis and Characterization of MnO₂ Nanoparticles

The MnO₂ NPs were successfully synthesized and used as carriers for TGF- β 3 delivery. The TEM images of the MnO₂ NPs clearly show the spherical morphology and hollow structure of the product, and the thickness of the MnO₂ shell was approximately 15 nm (Figure 1A). The corresponding EDS spectrum proved the presence of the Mn and O elements derived from MnO₂ and also confirmed the hollow structure of MnO₂ without element Si (Figure 1B). In addition, the cytotoxicity of the MnO₂ NPs was tested by CCK-8 assay, which found that the MnO₂ NPs did not exhibit obvious toxicity to NPCs, even at high concentrations up to 50 μ g/mL (Figure 1C). Hence, the MnO₂ NPs were used at a concentration of 50 μ g/mL in further experiments.

The Critical Examination of Controlled Drug Release

MnO₂ is known to be stable under neutral and basic conditions; however, it decomposes into Mn²⁺ under low pH.²⁸ A release test was performed to evaluate the degradation and loading of MnO₂ at different pH values (7.4 and 6.5) in the absence or presence of 100 μ M H₂O₂ for various treatment times lengths (Figure 2). The release curve shows that TGF- β 3 was continuously released from MnO₂ in a time-dependent manner. Compared with the slow drug release observed at pH 7.4, the rate of TGF- β 3 release was higher at pH 6.5. Furthermore, incubation with H₂O₂ at pH 6.5 further accelerated drug release by triggering the decomposition of the MnO₂ nanocarriers into Mn²⁺ ions.

In vitro Cellular Uptake of MnO₂ Nanoparticles

The endocytosis of NPs in NPCs was investigated by loading FITC-BSA into the MnO₂ NPs. As shown in Figure 3, the fluorescence signal of the FITC-BSA-loaded MnO₂ NPs was strong, indicating that the MnO₂ NPs had excellent drug-loading ability. In particular, the fluorescence signal was primarily located in the cytoplasm with some signal found in the nucleus. This confirmed the high cellular uptake of MnO₂ NPs.

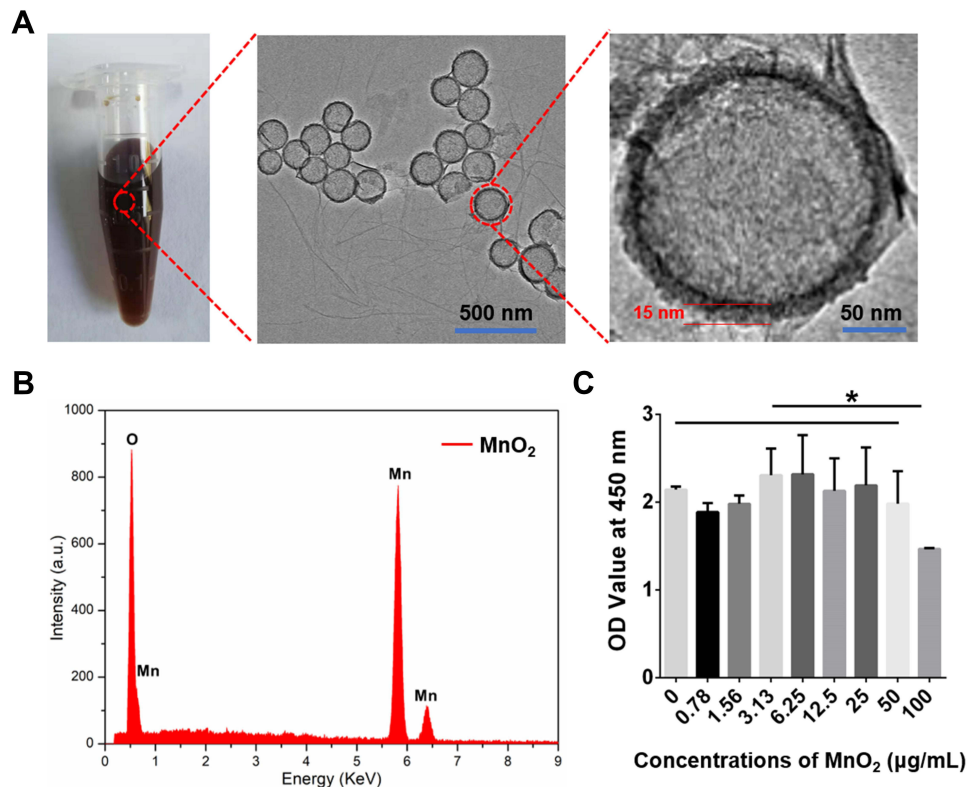


Figure 1 Synthesis and characterization of MnO₂ NPs. (A) Digital picture and TEM images of MnO₂ NPs. (B) EDS analysis of MnO₂ NPs. (C) Relative viabilities of NPCs treated with various concentrations of MnO₂ NPs for 24 h. *, $p < 0.05$.

Antioxidant Activity of TGF- β 3-Loaded MnO₂ Nanoparticles (TGF- β 3/MnO₂) Against H₂O₂

To investigate the ROS scavenging activity of TGF- β 3/MnO₂, the DCF fluorescence intensity was detected using an ROS assay kit. The ROS content increased after H₂O₂ treatment, but decreased following treatment with MnO₂ and TGF- β 3/MnO₂. However, treatment with TGF- β 3 did not significantly reverse H₂O₂-induced ROS production (Figure 4A). In addition, the expressions of the antioxidative genes SOD1, SOD2, and CAT were significantly increased in cells treated with MnO₂ and TGF- β 3/MnO₂ compared to cells treated with H₂O₂ and TGF- β 3 (Figure 4B–D). Hence, the antioxidant activity of TGF- β 3/MnO₂ was mainly attributed to MnO₂.

Anti-Apoptotic and Proliferative Effects of TGF- β 3/MnO₂ Against H₂O₂

We evaluated the anti-apoptotic effects of TGF- β 3/MnO₂ against H₂O₂ using the expression of the apoptotic gene BAX and the anti-apoptotic genes BCL2 and MCL1 in cultured NPCs. The expression of BAX was enhanced in H₂O₂-treated cells compared to the control NPCs. In contrast, the enhanced expression of the BAX gene was significantly reduced by treatment with TGF- β 3, MnO₂, or TGF- β 3/MnO₂, with TGF- β 3/MnO₂ producing the greatest decrease in BAX expression (Figure 5A). Compared to the cells treated with H₂O₂, the expression of BCL2 and MCL1 was significantly increased by treatment with TGF- β 3, MnO₂, or TGF- β 3/MnO₂, with TGF- β 3/MnO₂ resulting in the highest expressions (Figure 5B and C). Further, EdU assay showed that cell proliferation rate, represented by the percentage of EdU-positive cells, was decreased to 9.6% in H₂O₂-treated cells. Interestingly, this number was significantly increased to 17.6% and 18.5% in following treatment with MnO₂ and TGF- β 3, respectively, and it was markedly enhanced to 28.4% in the setting of TGF- β 3/MnO₂ (Figure 5D and E).

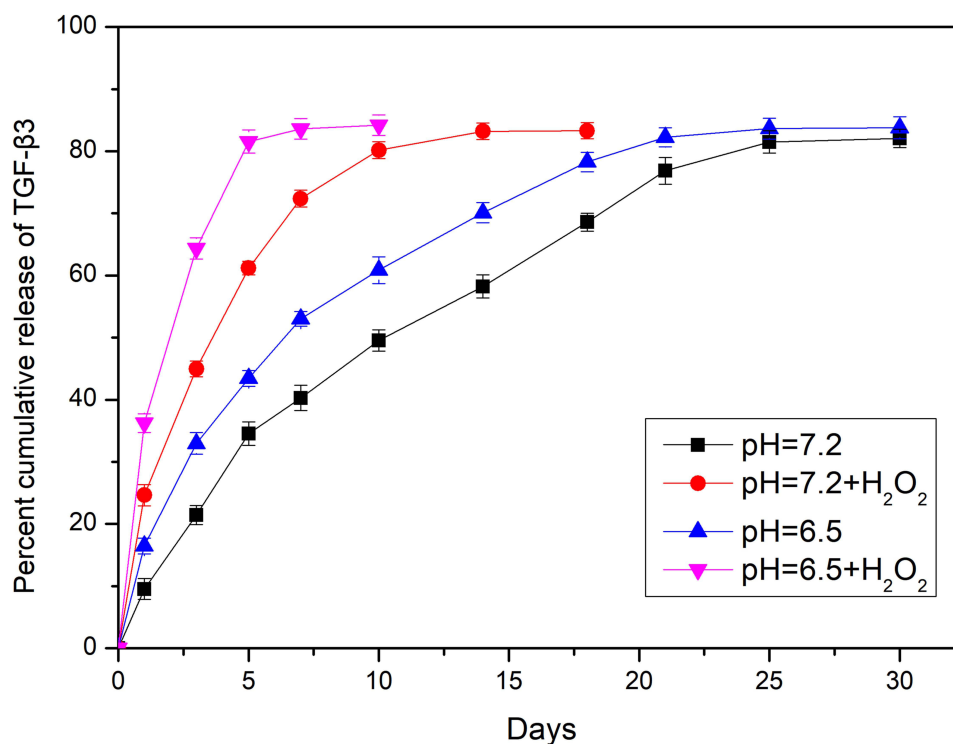


Figure 2 Nanoparticle decomposition and drug behaviors of TGF-β3/MnO₂. In vitro release of TGF-β3 from MnO₂ NPs at different pH values (7.4 and 6.5) in the absence or presence of 100 μM H₂O₂.

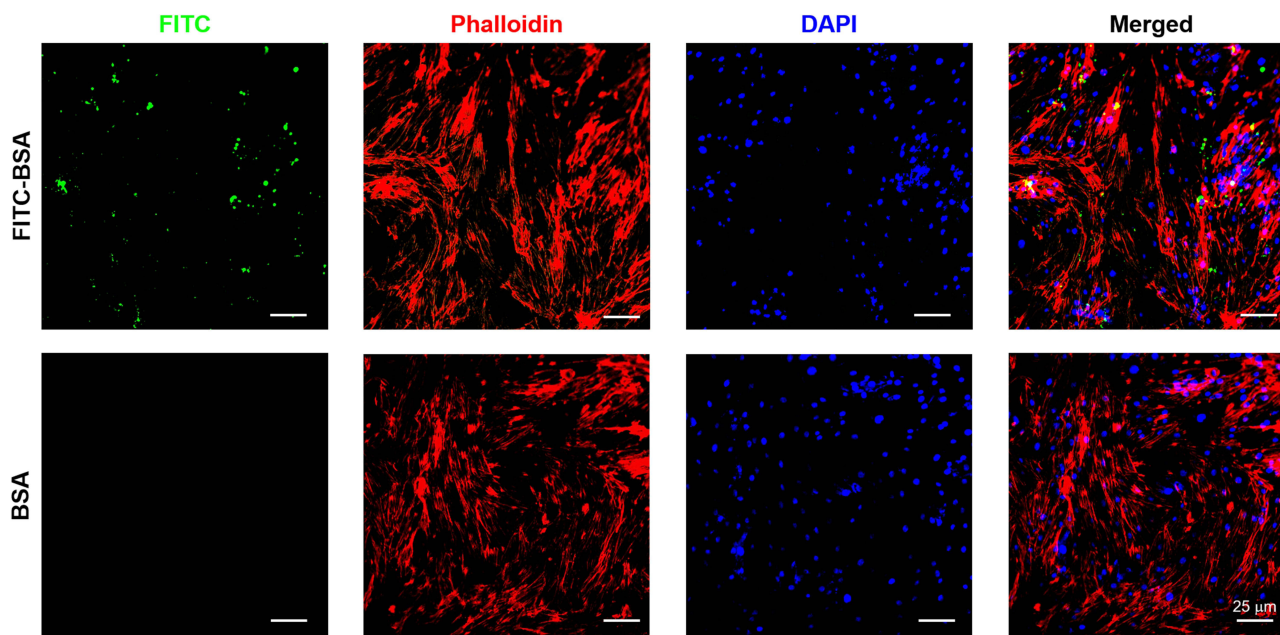


Figure 3 Representative images of NPC uptake of BSA/MnO₂ and FITC-BSA/MnO₂ for 12 h. Green, red and blue colors represent FITC-BSA/MnO₂, F-actin, and DAPI fluorescence, respectively.

Characterization of the Metabolic Effects of TGF-β3/MnO₂

The above results suggest that TGF-β3/MnO₂ exerted antioxidant, anti-apoptotic, and proliferative activities to protect cells from H₂O₂ damage. To further explore the effects of TGF-β3/MnO₂ on ECM synthesis in NPCs treated with H₂O₂, we conducted qPCR measurements to investigate the expressions of genes related to anabolism, inflammation, and

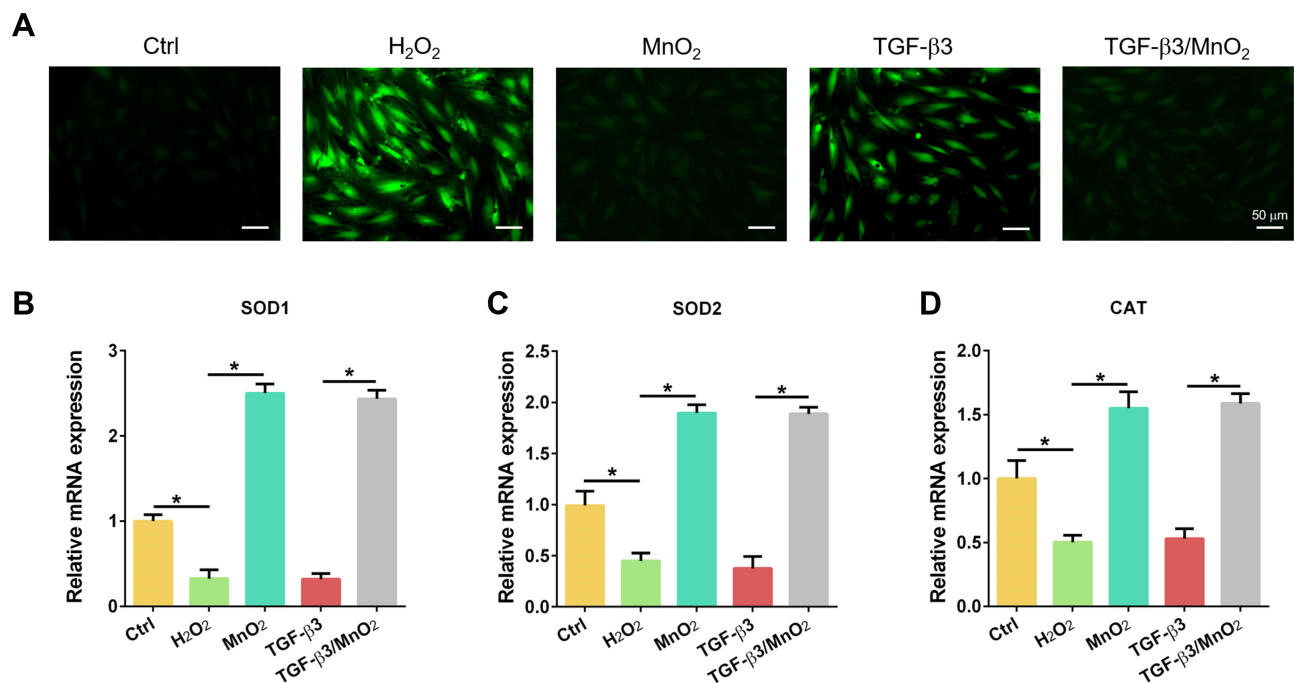


Figure 4 Antioxidant activity of TGF-β3/MnO₂ NPs. **(A)** Representative fluorescent images of NPCs stained with DCFH-DA in the Ctrl, H₂O₂, MnO₂, TGF-β3, and TGF-β3/MnO₂ groups, respectively. **(B–D)** qPCR analyses of the relative expression of the SOD1, SOD2, and CAT genes of the NPCs in Ctrl, H₂O₂, MnO₂, TGF-β3, and TGF-β3/MnO₂ groups, respectively. *, p<0.05.

catabolism. Of the studied treatments, TGF-β3/MnO₂ had the best ability to reverse the H₂O₂-induced expression of the ECM genes Col-II and ACAN (Figure 6A and B). Further, TGF-β3/MnO₂ almost completely blocked the stimulatory effect of H₂O₂ on the expressions of the pro-inflammatory enzymes COX-2 and iNOS (Figure 6C and D) and the catabolic genes MMP3 and Adamts5 (Figure 6E and F). Immunofluorescent experiments also confirmed that Col-II associated fluorescence intensity in the TGF-β3/MnO₂ group, was highest of the experimental groups (Figure 7A and B). Meanwhile, lower fluorescence intensity of iNOS was observed after TGF-β3/MnO₂ treatment (Figure 7C and D).

In vivo Evaluation of Intervertebral Disc Regeneration by TGF-β3/MnO₂

To assess the in vivo effect of TGF-β3/MnO₂ treatment, a rat disc puncture model was established. PBS, MnO₂, TGF-β3, or TGF-β3/MnO₂ was injected into the rat IVDs after they were punctured with a 21G needle. The therapeutic efficacy was evaluated based on changes in the gross appearance (Figure 8A) and MRI images (Figure 8B). After puncture, the gross appearance and T2-weighted MRI signal intensity of the IVDs were similar in the sham group and the group treated with TGF-β3/MnO₂. In contrast, discs treated with PBS, MnO₂, and TGF-β3 lost their signal, and water was observed (Figure 8C and D). The morphologies of the discs in each group were also evaluated with H&E (Figure 9A) and Safranin O-Fast Green staining (Figure 9B). In the sham group, the discs contained elliptical nucleus pulposus (NP), well-organized collagen lamellae, and a clear boundary between the annulus fibrosus (AF) and NP. From four to eight weeks after puncture, the size of the NP region and proteoglycan content decreased in the TGF-β3/MnO₂ group; however, these changes were relatively minor compared to the other experimental groups, and a clear tissue boundary between the AF and NP was still observed. In the PBS, MnO₂, and TGF-β3 groups, the discs displayed degenerative characteristics such as decreased NP size and disorganized collagen fibers in the inner AF. The histopathological scores of the TGF-β3/MnO₂ group were significantly lower after 4 weeks, which were closest to the Ctrl group. Conversely, the histopathological scores of the other experimental groups were significantly higher, a difference that were more obvious at week 8 (Figure 9C and D).

Finally, to verify the effectiveness of TGF-β3/MnO₂, the expressions of iNOS and Col-II in the IVD tissue were further evaluated using immunohistochemistry. The expression of iNOS was significantly lower in the TGF-β3/MnO₂

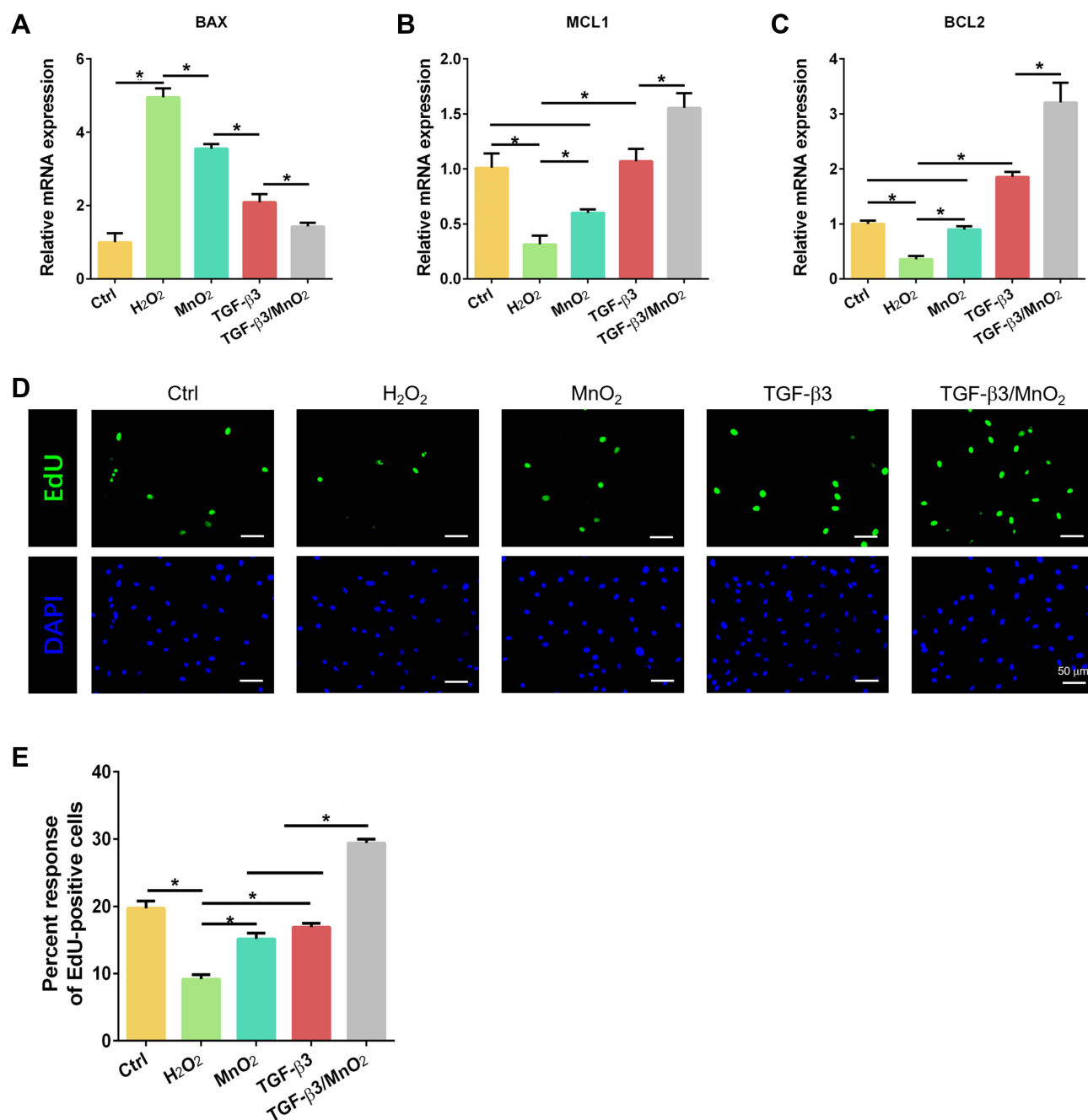


Figure 5 Anti-apoptotic and proliferative effects of TGF-β3/MnO₂. qPCR analyses of the relative expression of apoptotic (BAX) (A) and anti-apoptotic (MCL1 and BCL2) (B and C) genes of NPCs in the Ctrl, H₂O₂, MnO₂, TGF-β3, and TGF-β3/MnO₂ groups, respectively. (D) Representative images of EdU staining of NPCs in the Ctrl, H₂O₂, MnO₂, TGF-β3, and TGF-β3/MnO₂ groups, respectively. Green represents EdU-labeled proliferating cells and blue represents nuclei. (E) Quantification of the percentage of EdU-positive cells in the Ctrl, H₂O₂, MnO₂, TGF-β3, and TGF-β3/MnO₂ groups, respectively. *, p<0.05.

group than in the other experimental groups (Figure 10A). Conversely, the expression of Col-II, an important marker of ECM in the NP, was significantly higher in the TGF-β3/MnO₂ group than in the other experimental groups (Figure 10B). Semi-quantitative analysis of the staining further illustrated these differences (Figure 10C and D). Therefore, from a macroscopic perspective, the in vivo experimental results indicate that the TGF-β3/MnO₂ group had superior MRI signal and gross appearance compared with the other experimental groups. At the microscopic level, immunohistochemical staining revealed more residual NP, lower iNOS expression, and significantly higher Col-II expression in the TGF-β3/MnO₂ group. This indicates that the imbalance in ECM synthesis in IDD, which is one of the main causes of

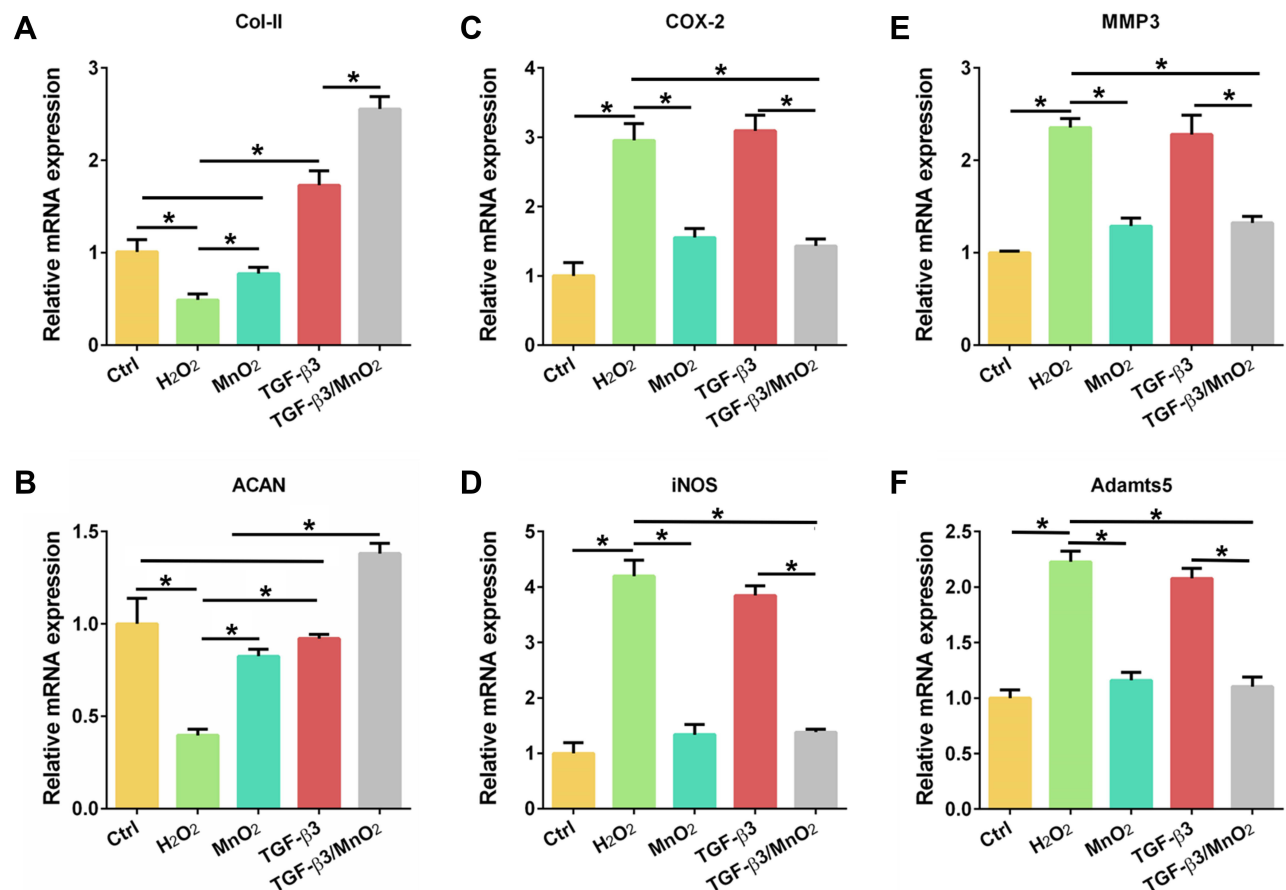


Figure 6 TGF-β₃/MnO₂ regulating the ECM metabolic balance of NPCs in vitro. qPCR analyses of the relative expression of anabolic (Col-II and ACAN) (**A** and **B**), pro-inflammatory (COX-2 and iNOS) (**C** and **D**), and catabolic (MMP3 and Adamts5) (**E** and **F**) genes in the NPCs of the Ctrl, H₂O₂, MnO₂, TGF-β₃, and TGF-β₃/MnO₂ groups, respectively. *, p<0.05.

the loss of IVD function, can be reversed, thereby delaying the progression of IVD degeneration. This effect was attributed to the ability of the MnO₂ NPs to create an appropriate microenvironment/vehicle for TGF-β₃ delivery to the IVDs. Moreover, TGF-β₃ delivered via the MnO₂ system effectively promoted cell proliferation and inhibited ECM degradation by reducing the acidity and scavenging ROS of the IVD microenvironment.

Discussion

We have proposed a novel strategy for IDD treatment using a MnO₂ nanoplatform that effectively releases TGF-β₃ in response to the acidic microenvironment produced by IDD. This novel nanoplatform can also decrease ROS accumulation to further promote cell survival and endogenous repair. The mechanisms and effectiveness of the proposed therapeutic system were validated both in vitro using rat NPCs and in vivo using a rat IDD model. Growing evidence suggests that the progression of IDD is accompanied by a pronounced decline in cell density.²⁹ The IVD is an avascular organ with a small cell population and a limited nutrient supply, resulting in poor endogenous repair capability.^{30,31} During aging and degeneration, excessive cellular senescence and death prevent the natural repair processes from occurring, exacerbating IDD.^{32,33} Anti-senescent therapy appears to have a curative effect on IDD.^{34,35}

Regenerative medicine has emerged as a promising option for the prevention or even reversal of disc degeneration.³⁶ Growth factors, which are an important component of regenerative medicine, act as mediators of the healing processes and represent potential molecular targets for stimulating and guiding regeneration.³⁷ TGF-β₃ plays an essential role in cell differentiation, cell adhesion, and ECM formation; TGF-β₃ has been shown to promote the repair of cartilaginous

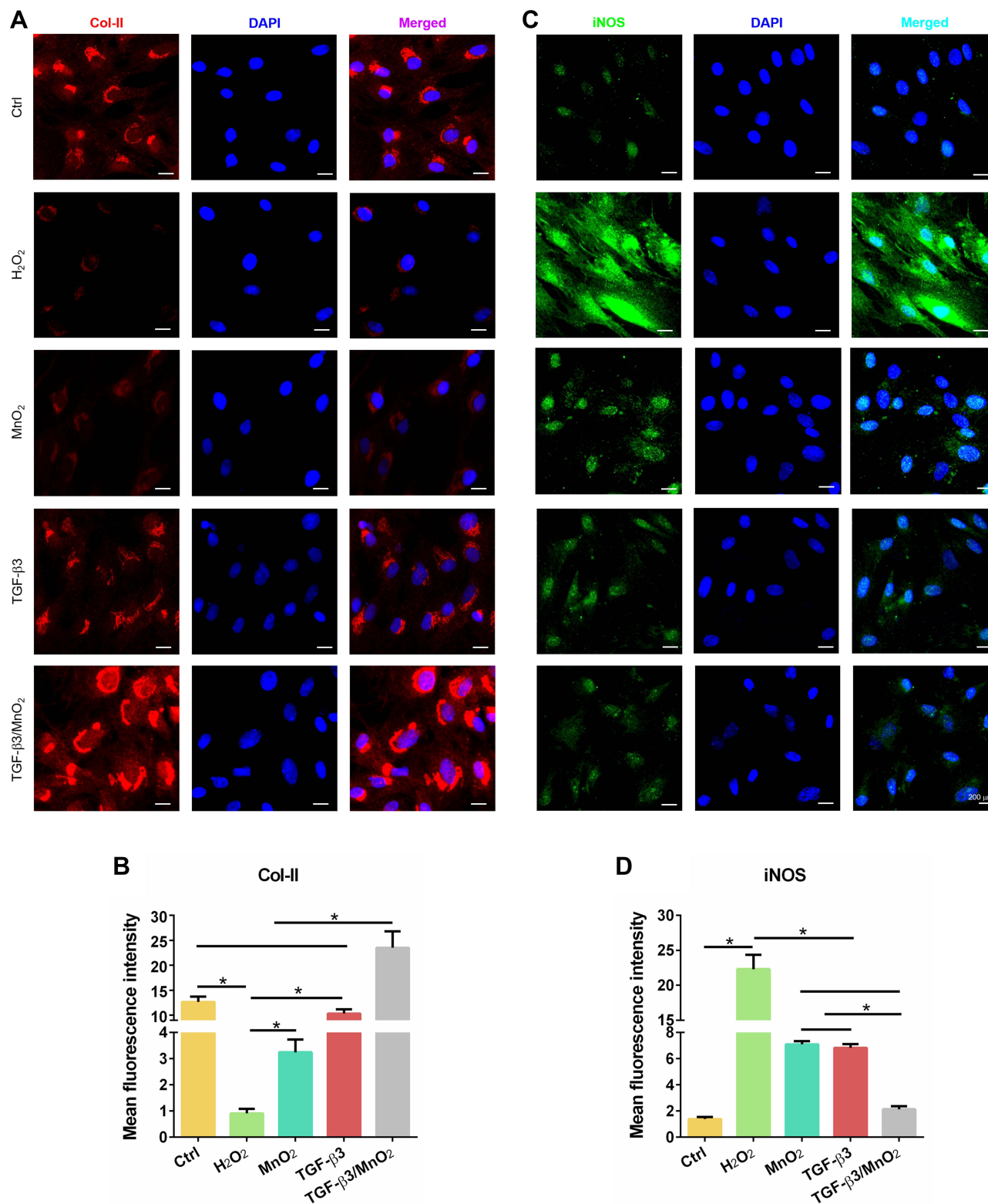


Figure 7 Immunofluorescent analysis of Col-II and iNOS expression in NPCs. Representative images of the immunofluorescence of Col-II (A) with semi-quantitative analysis (B) and iNOS (C) with semi-quantitative analysis (D) in the NPCs of the Ctrl, H₂O₂, MnO₂, TGF-β3, and TGF-β3/MnO₂ groups, respectively. Red, green and blue colors indicate Col-II protein, iNOS protein and DAPI fluorescence, respectively. *, p<0.05.

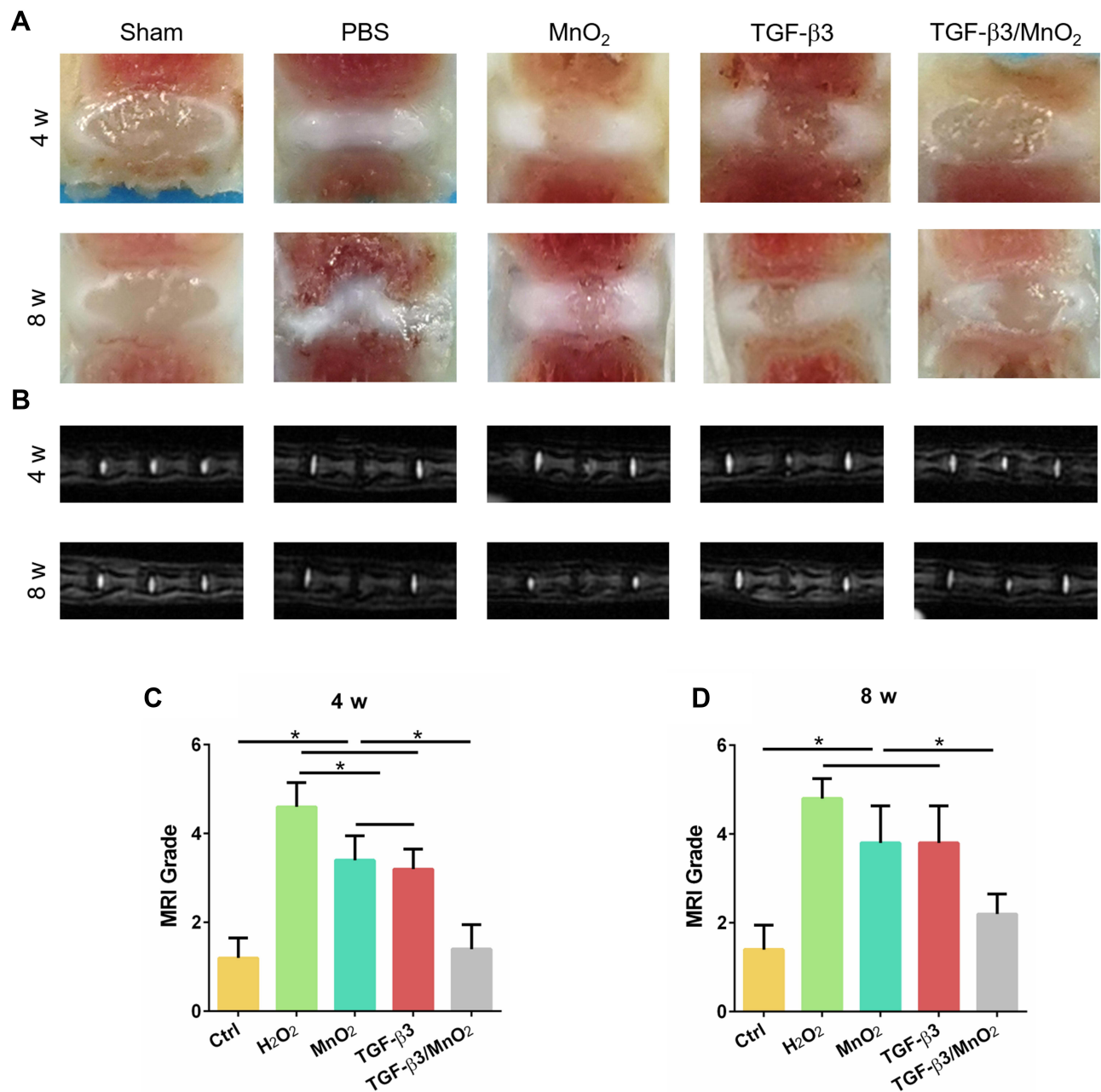


Figure 8 Evaluation of disc degeneration with T2-weighted MRI and gross appearance. Representative images of disc gross appearance (A) and MRI signal intensity (B) at 4 and 8 weeks. Changes in MRI grade at 4 and 8 weeks after surgery (C and D). *, $p < 0.05$.

organs including IVDs and upregulate the expressions of aggrecan and type II collagen.³⁸ Peck et al reported that TGF-β₃ enhanced cell survival and ECM synthesis of mesenchymal stem cells in low-oxygen and nutrient-limited microenvironments.³⁹ Ashraf et al reported that TGF-β₃ enhanced the ability of NPCs to form tissues, in part by decreasing cell death.⁴⁰ Consistent with the results of the present study, TGF-β₃ treatment blocked the inhibitory effect of H₂O₂ on NPC proliferation, likely by suppressing the apoptotic gene BAX and upregulating the proliferative genes MCL1 and BCL2. Further, TGF-β₃ alleviated the H₂O₂-induced expression of ECM genes (ACAN and Col-II) and partly blocked the stimulatory effect of H₂O₂ on the expression of catabolic (MMP3 and Adamts5) and inflammatory genes (COX-2 and iNOS). Interestingly, the protective effect of TGF-β₃ against H₂O₂ damage in NPCs was independent of the inhibition of oxidative stress, as evidenced by the lack of any effect of TGF-β₃ on intracellular ROS and antioxidant

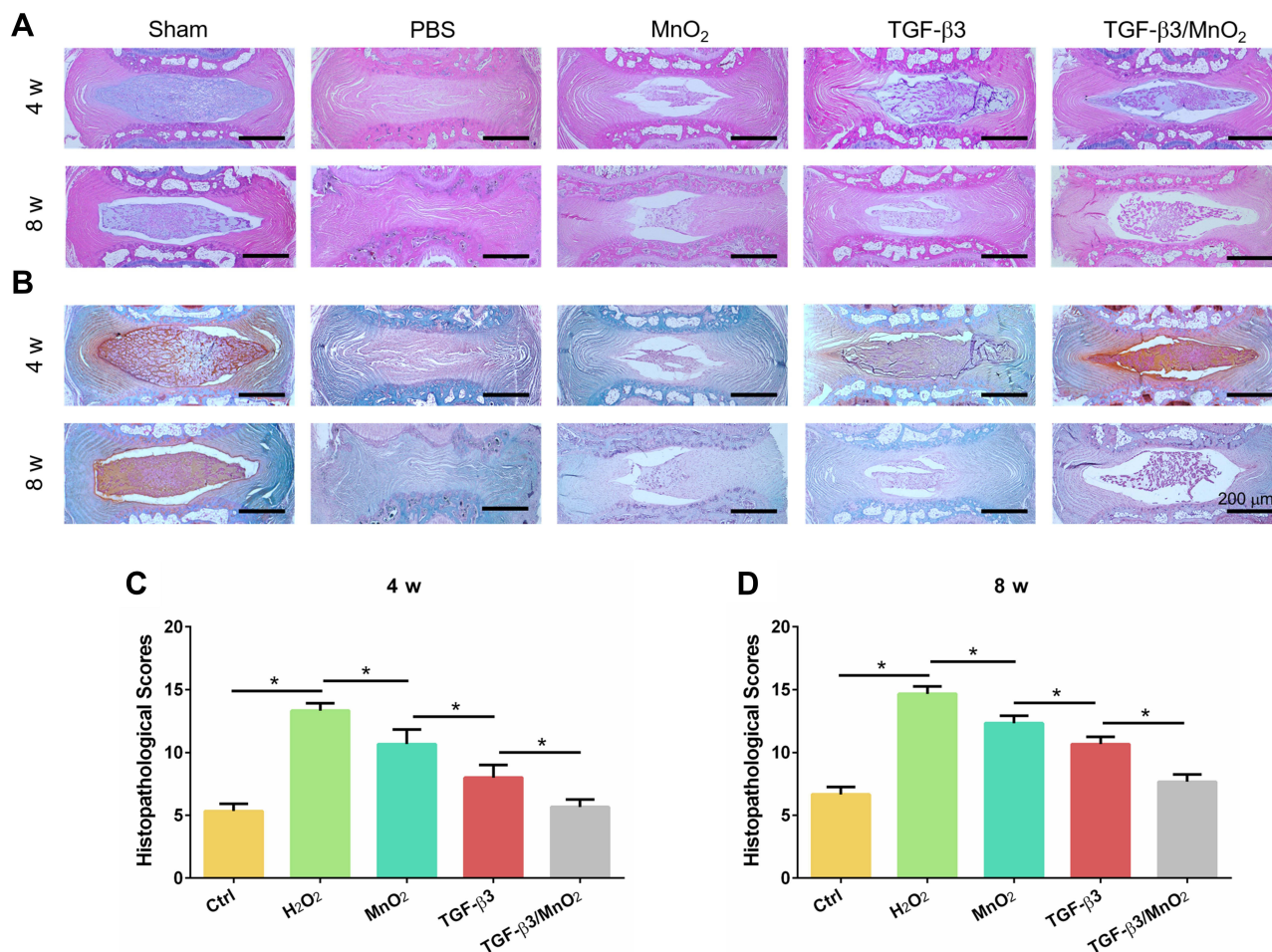


Figure 9 Histopathological evaluation in vivo. H&E (A) and Safranin O-Fast Green (B) images of IVDs in the rat caudal vertebrae at 4 and 8 weeks. The histopathological scores of different groups at 4 and 8 weeks after surgery (C and D). *, $p < 0.05$.

genes. In a rat model of IDD induced by needle puncture, the reductions in water and Col-II contents were attenuated by TGF- β 3 treatment, which is consistent with the recovery of the MRI signal at four weeks after injection. Regrettably, the effectiveness of TGF- β 3 was diminished at 8 weeks after injection, as evidenced by decreased in NP area and ECM content. This is likely because growth factors are prone to degradation in the body.⁴¹ Furthermore, the iNOS expression was higher in the group treated with TGF- β 3 alone compared to the sham group at both time points (4 w and 8 w). This may represent an increased inflammatory response and persistent oxidative stress within the IDD microenvironment, which may be another important reason why the positive effects of TGF- β 3 attenuate over time.

Increasing evidence suggests that the harsh disc microenvironment inhibits the self-healing processes of degenerating IVDs and restricts the capacity for external intervention.^{33,42} Oxidative stress has been identified as a major risk component of pathological mechanism behind IDD.^{43,44} Oxidative stress increases the concentration of ROS, which is closely related to cell senescence and apoptosis.⁴⁵ Further, oxidative stress enhances the degradation of the ECM and the inflammatory response in IVD cells and damages the mechanical function of the IVDs.^{8,46} These effects accelerate the progress of IDD and lead to low back pain. Disc degeneration has long been associated with increased acidity.⁴⁷ The pH value of normal discs is 7.2, while the pH in severely degenerated discs is 6.2.^{48,49} A normal pH is necessary to maintain cellular functions, while an excessively acidic environment significantly inhibits cell viability and matrix synthesis.⁵⁰ Gilbert et al reported that the increased pH was associated with decreased NPC proliferation and vitality, a shift towards matrix catabolism, and an increased expression of proinflammatory cytokines and pain-related factors.⁵¹ Therefore,

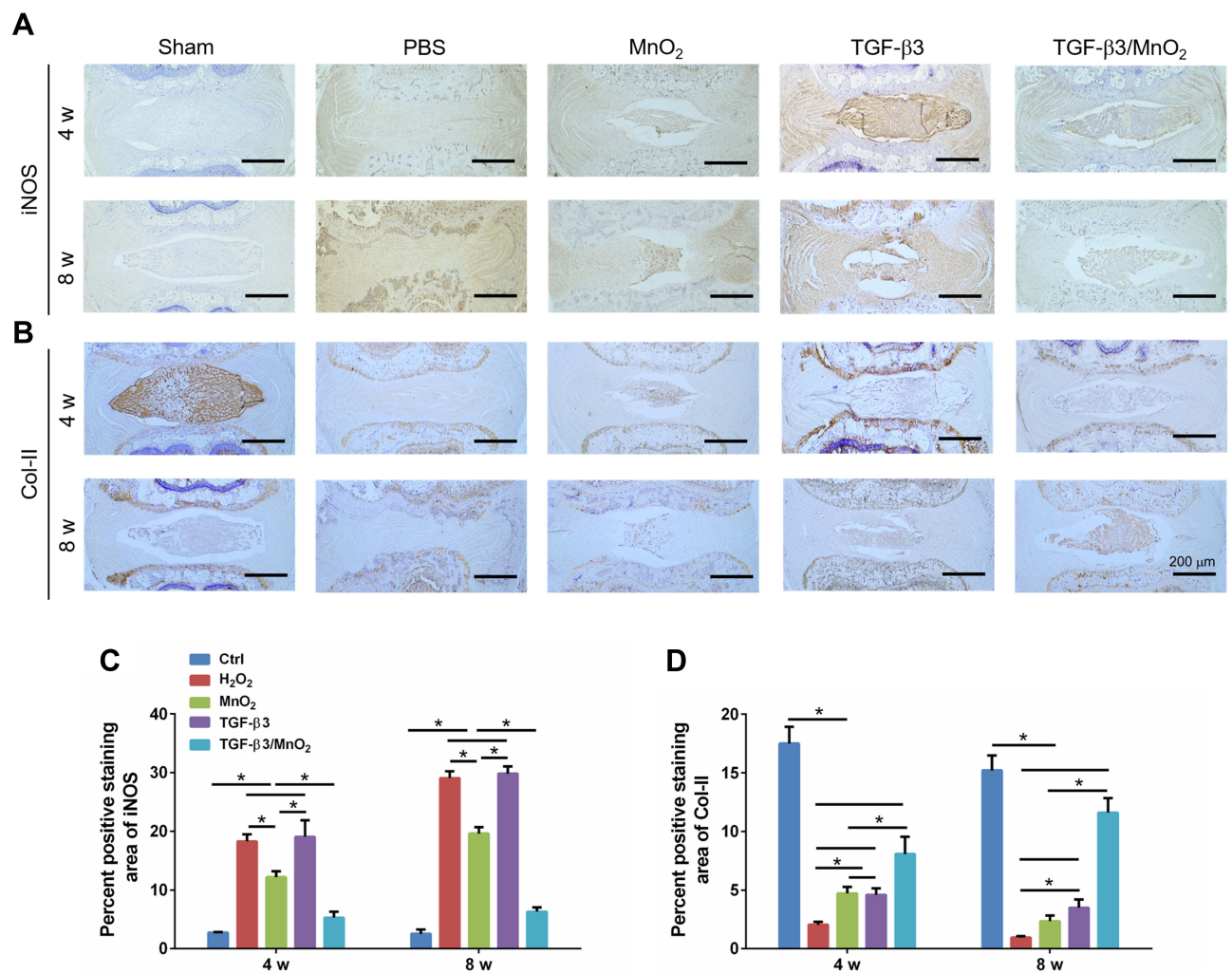


Figure 10 Immunohistochemical analysis of iNOS and Col-II expression in each group. Representative images of the immunohistochemical staining of iNOS (A) and Col-II (B) at 4 and 8 weeks after surgery, and the semi-quantitative analysis of iNOS (C) and COL-II (D) at these timepoints. *, $p < 0.05$.

targeting oxidative stress or acidity to improve the harsh microenvironment of disc degeneration may provide a new strategy for IDD treatment.

Based on the above considerations, MnO₂ nanostructures that are decomposed in the presence of H⁺ or glutathione have attracted our attention.⁵² MnO₂ nanostructures are also able to trigger the decomposition of H₂O₂ into water and oxygen.⁵³ These characteristics enhance the therapeutic potential of the nanostructure, in particular as anti-tumor and anti-osteoarthritis vectors.^{54,55} However, to the best of our knowledge, MnO₂ nanostructures have not yet been reported as a strategy for IDD therapy. In this study, we developed an intelligent nanoplatform based on MnO₂ NPs for TGF-β3 delivery. The nanoplatform exhibited an ultrasensitive pH-triggered release and H₂O₂-responsive oxygen generation to relieve IVD hypoxia and reduce oxidative injury, resulting in long-term therapeutic effects. We successfully synthesized spherical MnO₂ NPs with hollow structures. The NPs exhibited no obvious toxicity to the NPCs, even at high concentrations up to 50 μg/mL. The NPs were highly effective at drug loading. The encapsulated drug was precisely and controllably released upon exposure to H⁺ or H₂O₂. In vitro experiments demonstrated that TGF-β3/MnO₂ had antioxidant and anti-apoptosis effects and promoted cell proliferation. Although TGF-β3 did not increase the antioxidant capacity of MnO₂, the proliferative effect of TGF-β3 was enhanced by MnO₂. There was increased production of ECM components (eg, ACAN and Col-II) in the presence of H₂O₂ in cells treated with TGF-β3/MnO₂ compared to those treated with TGF-β3 alone. We hypothesized that the enhanced effects of TGF-β3 in the setting of MnO₂ may be related

to the elimination of H_2O_2 by MnO_2 , resulting in a better environment for cell survival. This effect may be derived from the reduction in inflammatory factors and catabolic makers.

To further investigate the role of TGF- β 3/ MnO_2 in vivo, an IDD model was established in rats by needle puncture with half penetration. Needle puncture is the most common method used to establish injury models because of its repeatability and short-term degenerative changes.⁵⁶ Our in vivo results showed that needle puncture induced rapid and severe disc degeneration, as indicated by the disappearance of the nucleus pulposus area and the imbalanced ECM. These altered morphological features were almost recovered at four weeks after treatment with TGF- β 3/ MnO_2 . Further, the MRI signal intensity and nucleus area were larger in the TGF- β 3/ MnO_2 group compared to the TGF- β 3 and MnO_2 groups. Additionally, TGF- β 3/ MnO_2 effectively slowed Col-II degradation and iNOS expression for up to eight weeks after treatment, which was not observed in the TGF- β 3 and MnO_2 groups. These findings reveal that MnO_2 contributes to eliminating oxidative stress and controlling the release of TGF- β 3, and the latter promoted cell survival, ECM deposition and enhanced endogenous repair.

The present study has some limitations. First, we only examined the effects of TGF- β 3/ MnO_2 on the rat IDD model for eight weeks. A longer study period is needed to evaluate the long-term efficacy of the nanopatform. Second, an upright model that is more similar to a human IDD should be used to further validate the results obtained in the rat IDD model. Third, the use of PBS solution as a vehicle increases the possibility of leakage. Thus, a better vehicle such as a hydrogel should be developed to improve drug bioavailability and avoid burst drug release.

Conclusion

In summary, we fabricated hollow mesoporous MnO_2 NPs loaded with TGF- β 3 as a multifunctional drug delivery system that is responsive to H^+ and H_2O_2 in the IDD microenvironment. This nanopatform can modulate the microenvironment to prolong the effects of TGF- β 3, which achieved well persistent influence in IDD injury. Further studies will be needed to explore some suitable vehicles to enhance the curative effect and longer treatment periods to confirm the long-term efficacy of the nanopatform. This injectable nanopatform for controlled drug release provides a new strategy for tissue regeneration under local oxidative stress and acidic microenvironments.

Acknowledgments

This study was supported by the people's livelihood Science and Technology Plan of Suzhou Municipal Government to Dr. Lifan Zhu (SS202090) and Ke Jiao Xing Wei Plan of Wujiang District (WWK202006) to Dr. Lifan Zhu.

Disclosure

No potential conflict of interest was reported by the authors.

References

1. Bonnevie E, Gullbrand S, Ashinsky B, et al. Aberrant mechanosensing in injured intervertebral discs as a result of boundary-constraint disruption and residual-strain loss. *Nat Biomed Eng.* 2019;3(12):998–1008. doi:10.1038/s41551-019-0458-4
2. Ji M, Jiang H, Zhang X, et al. Preclinical development of a microRNA-based therapy for intervertebral disc degeneration. *Nat Commun.* 2018;9(1):5051. doi:10.1038/s41467-018-07360-1
3. Schwarzer A, Aprill C, Derby R, Fortin J, Kine G, Bogduk N. The prevalence and clinical features of internal disc disruption in patients with chronic low back pain. *Spine.* 1995;20(17):1878–1883. doi:10.1097/00007632-199509000-00007
4. Wang S, Rui Y, Lu J, Wang C. Cell and molecular biology of intervertebral disc degeneration: current understanding and implications for potential therapeutic strategies. *Cell Prolif.* 2014;47(5):381–390. doi:10.1111/cpr.12121
5. Le Maitre C, Freemont A, Hoyland J. Accelerated cellular senescence in degenerate intervertebral discs: a possible role in the pathogenesis of intervertebral disc degeneration. *Arthritis Res Ther.* 2007;9(3):R45. doi:10.1186/ar2198
6. Zhao C, Jiang L, Dai L. Programmed cell death in intervertebral disc degeneration. *Apoptosis.* 2006;11(12):2079–2088. doi:10.1007/s10495-006-0290-7
7. Feng C, Liu H, Yang Y, Huang B, Zhou Y. Growth and differentiation factor-5 contributes to the structural and functional maintenance of the intervertebral disc. *Cell Physiol Biochem.* 2015;35(1):1–16. doi:10.1159/000369670
8. Feng C, Yang M, Lan M, et al. ROS: crucial intermediators in the pathogenesis of intervertebral disc degeneration. *Oxid Med Cell Longev.* 2017;2017:5601593. doi:10.1155/2017/5601593
9. Wang F, Shi R, Cai F, Wang Y, Wu X. Stem cell approaches to intervertebral disc regeneration: obstacles from the disc microenvironment. *Stem Cells Dev.* 2015;24(21):2479–2495. doi:10.1089/scd.2015.0158

10. Roger Y, Sydow S, Burmeister L, Menzel H, Hoffmann A. Sustained release of TGF- β from polysaccharide nanoparticles induces chondrogenic differentiation of human mesenchymal stromal cells. *Colloids Surf B Biointerfaces*. 2020;189:110843. doi:10.1016/j.colsurfb.2020.110843
11. Kimbrough-Allah M, Millena A, Khan S. Differential role of PTEN in transforming growth factor β (TGF- β) effects on proliferation and migration in prostate cancer cells. *Prostate*. 2018;78(5):377–389. doi:10.1002/pros.23482
12. Kazemnejad S, Khanmohammadi M, Mobini S, et al. Comparative repair capacity of knee osteochondral defects using regenerated silk fiber scaffolds and fibrin glue with/without autologous chondrocytes during 36 weeks in rabbit model. *Cell Tissue Res*. 2016;364(3):559–572. doi:10.1007/s00441-015-2355-9
13. Ma X, Ma X, Qian W, Zhao H, Ding J, Zhao T. Co-culture of adipose-derived stem cells and chondrocytes with transforming growth factor-beta 3 promotes chondrogenic differentiation. *J Craniofac Surg*. 2020;31(8):2355–2359. doi:10.1097/SCS.00000000000006748
14. Haberstroh K, Enz A, Zenclussen M, et al. Human intervertebral disc-derived cells are recruited by human serum and form nucleus pulposus-like tissue upon stimulation with TGF-beta3 or hyaluronan in vitro. *Tissue Cell*. 2009;41(6):414–420. doi:10.1016/j.tice.2009.05.006
15. Risbud M, Di Martino A, Guttapalli A, et al. Toward an optimum system for intervertebral disc organ culture: TGF-beta 3 enhances nucleus pulposus and annulus fibrosus survival and function through modulation of TGF-beta-R expression and ERK signaling. *Spine*. 2006;31(8):884–890. doi:10.1097/01.brs.0000209335.57767.b5
16. Mitchell M, Billingsley M, Haley R, Wechsler M, Peppas N, Langer R. Engineering precision nanoparticles for drug delivery. *Nat Rev Drug Discov*. 2021;20(2):101–124. doi:10.1038/s41573-020-0090-8
17. Blanco E, Shen H, Ferrari M. Principles of nanoparticle design for overcoming biological barriers to drug delivery. *Nat Biotechnol*. 2015;33(9):941–951. doi:10.1038/nbt.3330
18. Chang C, Qiu J, O'Sullivan D, et al. Metabolic competition in the tumor microenvironment is a driver of cancer progression. *Cell*. 2015;162(6):1229–1241. doi:10.1016/j.cell.2015.08.016
19. Ansari M, Ahmad N, Haqqi T. Oxidative stress and inflammation in osteoarthritis pathogenesis: role of polyphenols. *Biomed Pharmacother*. 2020;129:110452. doi:10.1016/j.biopha.2020.110452
20. Jiang L, Yuan F, Yin X, Dong J. Responses and adaptations of intervertebral disc cells to microenvironmental stress: a possible central role of autophagy in the adaptive mechanism. *Connect Tissue Res*. 2014;55(5–6):311–321. doi:10.3109/03008207.2014.942419
21. Yang G, Xu L, Chao Y, et al. Hollow MnO as a tumor-microenvironment-responsive biodegradable nano-platform for combination therapy favoring antitumor immune responses. *Nat Commun*. 2017;8(1):902. doi:10.1038/s41467-017-01050-0
22. Kumar S, Adjei IM, Brown SB, Liseth O, Sharma B. Manganese dioxide nanoparticles protect cartilage from inflammation-induced oxidative stress. *Biomaterials*. 2019;224:119467. doi:10.1016/j.biomaterials.2019.119467
23. Zhang G, Deng Y, Xie Q, et al. Sirtuins and intervertebral disc degeneration: roles in inflammation, oxidative stress, and mitochondrial function. *Clin Chim Acta*. 2020;508:33–42. doi:10.1016/j.cca.2020.04.016
24. Che H, Li J, Li Y, et al. p16 deficiency attenuates intervertebral disc degeneration by adjusting oxidative stress and nucleus pulposus cell cycle. *eLife*. 2020;9. DOI:10.7554/eLife.52570
25. Zeng W, Zhang H, Deng Y, Jiang A, Mei L. Dual-response oxygen-generating MnO₂ nanoparticles with polydopamine modification for combined photothermal-photodynamic therapy. *Chem Eng J*. 2020;389:124494. doi:10.1016/j.cej.2020.124494
26. Pfirrmann C, Metzdorf A, Zanetti M, Hodler J, Boos N. Magnetic resonance classification of lumbar intervertebral disc degeneration. *Spine*. 2001;26(17):1873–1878. doi:10.1097/00007632-200109010-00011
27. Masuda K, Aota Y, Muehleman C, et al. A novel rabbit model of mild, reproducible disc degeneration by an annulus needle puncture: correlation between the degree of disc injury and radiological and histological appearances of disc degeneration. *Spine*. 2005;30(1):5–14. doi:10.1097/01.brs.0000148152.04401.20
28. Wang X, Niu D, Wu Q, et al. Iron oxide/manganese oxide co-loaded hybrid nanogels as pH-responsive magnetic resonance contrast agents. *Biomaterials*. 2015;53:349–357. doi:10.1016/j.biomaterials.2015.02.101
29. Wang F, Cai F, Shi R, Wang X, Wu X. Aging and age related stresses: a senescence mechanism of intervertebral disc degeneration. *Osteoarthritis Cartilage*. 2016;24(3):398–408. doi:10.1016/j.joca.2015.09.019
30. Grunhagen T, Shirazi-Adl A, Fairbank J, Urban J. Intervertebral disk nutrition: a review of factors influencing concentrations of nutrients and metabolites. *Orthop Clin North Am*. 2011;42(4):465–477. doi:10.1016/j.ocl.2011.07.010
31. Li Z, Peroglio M, Alini M, Grad S. Potential and limitations of intervertebral disc endogenous repair. *Curr Stem Cell Res Ther*. 2015;10(4):329–338. doi:10.2174/1574888X10666150305105114
32. Vergroesen P, Kingma I, Emanuel K, et al. Mechanics and biology in intervertebral disc degeneration: a vicious circle. *Osteoarthritis Cartilage*. 2015;23(7):1057–1070. doi:10.1016/j.joca.2015.03.028
33. Ma K, Chen S, Li Z, et al. Mechanisms of endogenous repair failure during intervertebral disc degeneration. *Osteoarthritis Cartilage*. 2019;27(1):41–48. doi:10.1016/j.joca.2018.08.021
34. Yi W, Lan H, Wen Y, et al. HO-1 overexpression alleviates senescence by inducing autophagy via the mitochondrial route in human nucleus pulposus cells. *J Cell Physiol*. 2020;235(11):8402–8415. doi:10.1002/jcp.29684
35. Chen J, Xie J, Jin M, et al. Sirt6 overexpression suppresses senescence and apoptosis of nucleus pulposus cells by inducing autophagy in a model of intervertebral disc degeneration. *Cell Death Dis*. 2018;9(2):56. doi:10.1038/s41419-017-0085-5
36. Henry N, Clouet J, Le Bideau J, Le Visage C, Guicheux J. Innovative strategies for intervertebral disc regenerative medicine: from cell therapies to multiscale delivery systems. *Biotechnol Adv*. 2018;36(1):281–294. doi:10.1016/j.biotechadv.2017.11.009
37. Frapin L, Clouet J, Chédeville C, et al. Controlled release of biological factors for endogenous progenitor cell migration and intervertebral disc extracellular matrix remodelling. *Biomaterials*. 2020;253:120107. doi:10.1016/j.biomaterials.2020.120107
38. Tao Y, Zhou X, Liang C, et al. TGF- β 3 and IGF-1 synergy ameliorates nucleus pulposus mesenchymal stem cell differentiation towards the nucleus pulposus cell type through MAPK/ERK signaling. *Growth Factors*. 2015;33:326–336. doi:10.3109/08977194.2015.1088532
39. Peck S, Bendigo J, Tobias J, et al. Hypoxic preconditioning enhances bone marrow-derived mesenchymal stem cell survival in a low oxygen and nutrient-limited 3D microenvironment. *Cartilage*. 2019;12(4):512–525.
40. Ashraf S, Chatoor K, Chong J, Pilliar R, Santerre P, Kandel R. Transforming growth factor β enhances tissue formation by passaged nucleus pulposus cells in vitro. *J Orthop Res*. 2020;38(2):438–449. doi:10.1002/jor.24476

41. Blanquer S, Grijpma D, Poot A. Delivery systems for the treatment of degenerated intervertebral discs. *Adv Drug Deliv Rev.* 2015;84:172–187. doi:10.1016/j.addr.2014.10.024
42. Sakai D, Andersson G. Stem cell therapy for intervertebral disc regeneration: obstacles and solutions. *Nat Rev Rheumatol.* 2015;11(4):243–256. doi:10.1038/nrrheum.2015.13
43. Han Y, Li X, Yan M, et al. Oxidative damage induces apoptosis and promotes calcification in disc cartilage endplate cell through ROS/MAPK/NF- κ B pathway: implications for disc degeneration. *Biochem Biophys Res Commun.* 2019;516(3):1026–1032. doi:10.1016/j.bbrc.2017.03.111
44. Song D, Ge J, Wang Y, et al. Tea polyphenol attenuates oxidative stress-induced degeneration of intervertebral discs by regulating the Keap1/Nrf2/ARE pathway. *Oxid Med Cell Longev.* 2021;2021:6684147. doi:10.1155/2021/6684147
45. Wang B, Ke W, Wang K, et al. Mechanosensitive ion channel piezo1 activated by matrix stiffness regulates oxidative stress-induced senescence and apoptosis in human intervertebral disc degeneration. *Oxid Med Cell Longev.* 2021;2021:8884922. doi:10.1155/2021/8884922
46. Suzuki S, Fujita N, Hosogane N, et al. Excessive reactive oxygen species are therapeutic targets for intervertebral disc degeneration. *Arthritis Res Ther.* 2015;17(1):316. doi:10.1186/s13075-015-0834-8
47. Razaq S, Wilkins R, Urban J. The effect of extracellular pH on matrix turnover by cells of the bovine nucleus pulposus. *Eur Spine J.* 2003;12(4):341–349. doi:10.1007/s00586-003-0582-3
48. Diamant B, Karlsson J, Nachemson A. Correlation between lactate levels and pH in discs of patients with lumbar rhizopathies. *Experientia.* 1968;24(12):1195–1196. doi:10.1007/BF02146615
49. Nachemson A. Intradiscal measurements of pH in patients with lumbar rhizopathies. *Acta Orthop Scand.* 1969;40(1):23–42. doi:10.3109/17453676908989482
50. Liu J, Tao H, Wang H, et al. Biological behavior of human nucleus pulposus mesenchymal stem cells in response to changes in the acidic environment during intervertebral disc degeneration. *Stem Cells Dev.* 2017;26(12):901–911. doi:10.1089/scd.2016.0314
51. Gilbert H, Hodson N, Baird P, Richardson S, Hoyland J. Acidic pH promotes intervertebral disc degeneration: acid-sensing ion channel –3 as a potential therapeutic target. *Sci Rep.* 2016;6:37360. doi:10.1038/srep37360
52. Fan W, Bu W, Shen B, et al. Intelligent MnO₂ nanosheets anchored with upconversion nanoprobes for concurrent pH-/H₂O₂-Responsive UCL imaging and oxygen-elevated synergetic therapy. *Adv Mater.* 2015;27(28):4155–4161. doi:10.1002/adma.201405141
53. Gordijo CR, Abbasi AZ, Amini MA, et al. Hybrid nanoparticles: design of hybrid MnO₂-Polymer-Lipid nanoparticles with tunable oxygen generation rates and tumor accumulation for cancer treatment. *Adv Funct Mater.* 2015;25(12):1857–1587.
54. Chen L, Tiwari SR, Zhang Y, Zhang J, Sun Y. Facile synthesis of hollow MnO₂ nanoparticles for reactive oxygen species scavenging in osteoarthritis. *ACS Biomater Sci Eng.* 2021;7(4):1686–1692. doi:10.1021/acsbomaterials.1c00005
55. Prasad P, Gordijo C, Abbasi A, et al. Multifunctional albumin-MnO₂ nanoparticles modulate solid tumor microenvironment by attenuating hypoxia, acidosis, vascular endothelial growth factor and enhance radiation response. *ACS nano.* 2014;8(4):3202–3212. doi:10.1021/nm405773r
56. Keorochana G, Johnson J, Taghavi C, et al. The effect of needle size inducing degeneration in the rat caudal disc: evaluation using radiograph, magnetic resonance imaging, histology, and immunohistochemistry. *Spine J.* 2010;10(11):1014–1023. doi:10.1016/j.spinee.2010.08.013

Publish your work in this journal

The International Journal of Nanomedicine is an international, peer-reviewed journal focusing on the application of nanotechnology in diagnostics, therapeutics, and drug delivery systems throughout the biomedical field. This journal is indexed on PubMed Central, MedLine, CAS, SciSearch[®], Current Contents[®]/Clinical Medicine, Journal Citation Reports/Science Edition, EMBase, Scopus and the Elsevier Bibliographic databases. The manuscript management system is completely online and includes a very quick and fair peer-review system, which is all easy to use. Visit <http://www.dovepress.com/testimonials.php> to read real quotes from published authors.

Submit your manuscript here: <https://www.dovepress.com/international-journal-of-nanomedicine-journal>